Letter

Scaling approach to nuclear structure in high-energy heavy-ion collisions

Jiangyong Jia [1,2,*] and Chunjian Zhang [1,†]
[1]*Department of Chemistry, Stony Brook University, Stony Brook, New York 11794, USA*
[2]*Physics Department, Brookhaven National Laboratory, Upton, New York 11976, USA*

(Received 16 December 2021; revised 17 August 2022; accepted 25 January 2023; published 14 February 2023)

In high-energy heavy-ion collisions, the initial condition of the produced quark-gluon plasma (QGP) and its evolution are sensitive to collective nuclear structure parameters describing the shape and radial profiles of the nuclei. We find a general scaling relation between these parameters and many experimental observables such as elliptic flow, triangular flow, and particle multiplicity distribution. In particular, the ratios of observables between two isobar systems depend only on the differences of these parameters, but not on the details of the final state interactions, hence offering a new way to constrain the QGP initial condition. Using this scaling relation, we show how the structure parameters of $^{96}_{44}$Ru and $^{96}_{40}$Zr conspire to produce the rich centrality dependences of these ratios, as measured by the STAR Collaboration. Our scaling approach demonstrates that isobar collisions are a precision tool to probe the initial condition of heavy-ion collisions, as well as the collective nuclear structures, including the neutron skin, of the atomic nuclei across energy scales.

DOI: 10.1103/PhysRevC.107.L021901

One main challenge in nuclear physics is to map out the shape and radial structure of the atomic nuclei and understand how they emerge from the interactions among the constituent nucleons [1,2]. Varying the number of nucleons along isotopic/isotonic chain often induces rich and nonmonotonic changes in the nuclear structure properties. In certain regions of nuclear chart, for example, even adding or subtracting a few nucleons can induce significant deformations and/or changes in the nuclear radius or neutron skin [3–6]. Experimental information on nuclear structure is primarily obtained by spectroscopic or scattering measurements at low energies. But studies show that nuclear structure can be probed in high-energy nuclear collisions at the BNL Relativistic HeavyIon Collider (RHIC) and the CERN Large Hadron Collider (LHC) [7–21], and experimental evidences have been observed [22–26].

The connection between nuclear structure and high-energy heavy-ion collisions is illustrated in Fig. 1. These collisions deposit a large amount of energy in the overlap region in the middle panel, forming a hot and dense quark-gluon plasma (QGP) [27]. Driven by large pressure gradients, the QGP undergoes a hydrodynamical expansion, converting the initial spatial anisotropies into momentum anisotropies of particles in the final state in the right panel. Observables describing the collective features of the particles in the final state, such as elliptic flow v_2, triangular flow v_3 and charged particle multiplicity $N_{\rm ch}$ are closely related to geometric features of the initial condition, ellipticity ε_2, triangularity ε_3, and number of participating nucleons $N_{\rm part}$, respectively. In fact, at energies reached at RHIC and the LHC, $\sqrt{s_{NN}} \geqslant 100$ GeV, these quantities are linearly-related $v_n \propto \varepsilon_n$ and $N_{\rm ch} \propto N_{\rm part}$ [28,29]. On the other hand, the shape and size of the initial condition are affected by the nucleon distribution in the colliding nuclei in the left panel, often described by a deformed Woods-Saxon (WS) density,

$$\rho(r,\theta,\phi) \propto \frac{1}{1+e^{[r-R_0(1+\beta_2 Y_2^0(\theta,\phi)+\beta_3 Y_3^0(\theta,\phi))]/a}}, \qquad (1)$$

containing four structure parameters: quadrupole deformation β_2 and octupole deformation β_3, half-density radius R_0, and surface diffuseness a [30]. The deformation β_2 (β_3) enhances the ε_2 (ε_3) in the initial condition [10,20,31]. A change in a influences ε_n and charge particle multiplicity distribution $p(N_{\rm part})$ [12,32]. Both a and R_0 were shown to have significant impact on the initial overlap area [33,34]. In more recent studies, these structure parameters are found to have much larger impact on multipoint correlators in both the initial and final state [35–37]. Understanding the role of nuclear structure can improve modeling of the initial condition, which currently limits the extraction of the transport properties of the QGP [38–40].

Due to the dominant role of the impact parameter, earlier studies focused on the most central collisions where the impact of nuclear structure can be easily identified. It is realized recently that the nuclear structure impact can be cleanly isolated over the full centrality range by comparing two isobaric collision systems [17,18]. Since isobar nuclei have the same mass number but different structures, deviation from unity of the ratio of any observable must originate from differences in the structure of the colliding nuclei, which impact the initial state of QGP and its final state evolution. Collisions of one such pair of isobar systems, ^{96}Ru + ^{96}Ru and ^{96}Zr + ^{96}Zr, have been performed at RHIC. Ratios of many observables are

*Corresponding author: jiangyong.jia@stonybrook.edu
†Corresponding author: chun-jian.zhang@stonybrook.edu

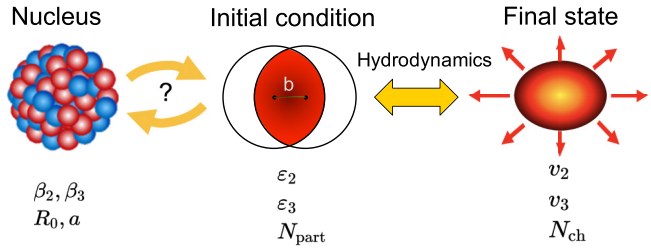

FIG. 1. Connection between collective nuclear structure (left), the initial condition (middle), and final state (right) of high-energy heavy-ion collisions, together with parameters describing the geometrical aspects for each phase (see text). Due to the extremely short nuclear crossing time $2R_0/\gamma \lesssim 0.1$ fm/c, the initial condition is well separated from the hydrodynamical evolution in the final state. The geometry of the initial condition depends on the impact parameter b and structure parameters.

found to show significant and centrality-dependent departures from unity [41]. The goal of this Letter is to explore the scaling behavior of these ratios with respect to the WS parameters in Eq. (1).

We illustrate this point using three heavy-ion observables, the $v_2(N_{\rm ch})$, $v_3(N_{\rm ch})$, and $p(N_{\rm ch})$, although the same idea applies to many other single-particle or two-particle observables. For small deformations and small variations of R_0 and a from their default reference values, the observable $\mathcal{O}$ has the following leading-order form:

$$\mathcal{O} \approx b_0 + b_1\beta_2^2 + b_2\beta_3^2 + b_3(R_0 - R_{0,\rm ref}) + b_4(a - a_{\rm ref}), \tag{2}$$

where b_0 is the value for spherical nuclei at some reference radius and diffuseness, and b_1–b_4 are centrality-dependent response coefficients that encode the final-state dynamics.[1] Most dependence on mass number is carried by b_0, while b_1–b_4 are expected to be weak functions of mass number. The ratio of $\mathcal{O}$ between ^{96}Ru+^{96}Ru and ^{96}Zr+^{96}Zr then has a simple scaling relation

$$R_{\mathcal{O}} \equiv \frac{\mathcal{O}_{\rm Ru}}{\mathcal{O}_{\rm Zr}} \approx 1 + c_1\Delta\beta_2^2 + c_2\Delta\beta_3^2 + c_3\Delta R_0 + c_4\Delta a, \tag{3}$$

where $\Delta\beta_n^2 = \beta_{n,\rm Ru}^2 - \beta_{n,\rm Zr}^2$, $\Delta R_0 = R_{0,\rm Ru} - R_{0,\rm Zr}$, $\Delta a = a_{\rm Ru} - a_{\rm Zr}$, and $c_n = b_n/b_0$. Two important insights can be drawn if Eq. (3) holds: 1) these ratios can only probe the difference in the WS parameters between the isobar nuclei, 2) the contributions are independent of each other among the WS parameters.

To verify this scaling relation, we simulate the dynamics of the QGP using the multiphase transport model (AMPT) [43]. The AMPT model describes collective flow data at RHIC and LHC [44,45] and was used to study the β_n dependence of v_n [18,46]. We use AMPT v2.26t5 in string-melting mode at $\sqrt{s_{NN}} = 200$ GeV with a partonic cross section of 3.0 mb [47,48]. We simulate generic isobar ^{96}X+^{96}X collisions covering a wide range of β_2, β_3, R_0, and a, including the default values assumed for ^{96}Ru and ^{96}Zr listed in Table I. Following Ref. [49], the default values are taken from Ref. [50] for R_0 or deduced from neutron skin data [51] for a. The default values of β_2 and β_3 are taken from Ref. [46]. The v_n are calculated using two-particle correlation method with hadrons of $0.2 < p_T < 2$ GeV and $|\eta| < 2$ [52]. The ratios are calculated as a function of $N_{\rm ch}$ instead of centrality, because the ratios calculated at the same $N_{\rm ch}$ have a good cancellation of nonflow contributions [53] and the final state effects [33].

TABLE I. Collective nuclear structure parameters for ^{96}Ru and ^{96}Zr and the differences.

Species	β_2	β_3	a	R_0
^{96}Ru	0.162	0	0.46 fm	5.09 fm
^{96}Zr	0.06	0.20	0.52 fm	5.02 fm
difference	$\Delta\beta_2^2$	$\Delta\beta_3^2$	Δa	ΔR_0
	0.0226	-0.04	-0.06 fm	0.07 fm

To explore the parametric dependence of the hydrodynamic response, the parameters are varied one at a time. The β_2 is changed from 0 to 0.1, 0.15, and 0.2; the β_3 is changed from 0 to 0.1, 0.2, and 0.25; the a is varied from 0.52 fm to 0.46 fm, 0.40 fm, and 0.34 fm; the R_0 is varied from 5.09 fm to 5.02 fm, 4.8 fm, and 4.5 fm. An independent sample is generated for each case and the v_2, v_3, and $p(N_{\rm ch})$ are calculated. The change in the ratios from unity, $R_{\mathcal{O}} - 1$, are scaled according to the actual differences between Ru and Zr listed in Table I. The results for all 12 cases (four parameters times three observables) as a function of $N_{\rm ch}$ are summarized in Fig. 2 [54].

One striking feature is the nearly perfect scaling of $R_{\mathcal{O}}$ over the wide range of parameter values studied. The shapes of these dependences reflect directly the response coefficients $c_n(N_{\rm ch})$ for each observable. The statistical uncertainties of c_n decrease for larger variations of the WS parameters, implying that the c_n can be determined more precisely by using a larger change of each parameter. This has the benefit of significantly reducing the number of events required in the hydrodynamic model simulation to achieve the desired precision, ideally suitable for the multi-system Bayesian global analyses of heavy-ion collisions [40,55].

All the WS parameters do not have the same influences on final state observables. In peripheral and midcentral collisions, the ratio $p(N_{\rm ch})_{\rm Ru}/p(N_{\rm ch})_{\rm Zr}$ is influenced mostly by the Δa and ΔR_0. In particular, the characteristic broad peak and nonmonotonic behavior of the ratio is a clear signature of the influence of Δa [49]. In the most central collisions, the ratio is sensitive to all four parameters. The influence of WS parameters on $v_{2,\rm Ru}/v_{2,\rm Zr}$ is richer: 1) in the most central collisions, the ratio is mainly dominated by $\Delta\beta_2^2$ and to a lesser extent by $\Delta\beta_3^2$; 2) in the near-central collisions, the ratio is influenced by a positive contribution from $\Delta\beta_2^2$ and a larger negative contribution from $\Delta\beta_3^2$; 3) in the midcentral and

[1]Note that the leading-order contribution from deformation appears as β_n^2 instead of β_n because these observables do not depend on the sign of β_n [20,42]. For higher-order correlators, such as skewness of p_T fluctuation and $v_n^2 - p_T$ correlation, the leading order term scales with β_n^3 [42].

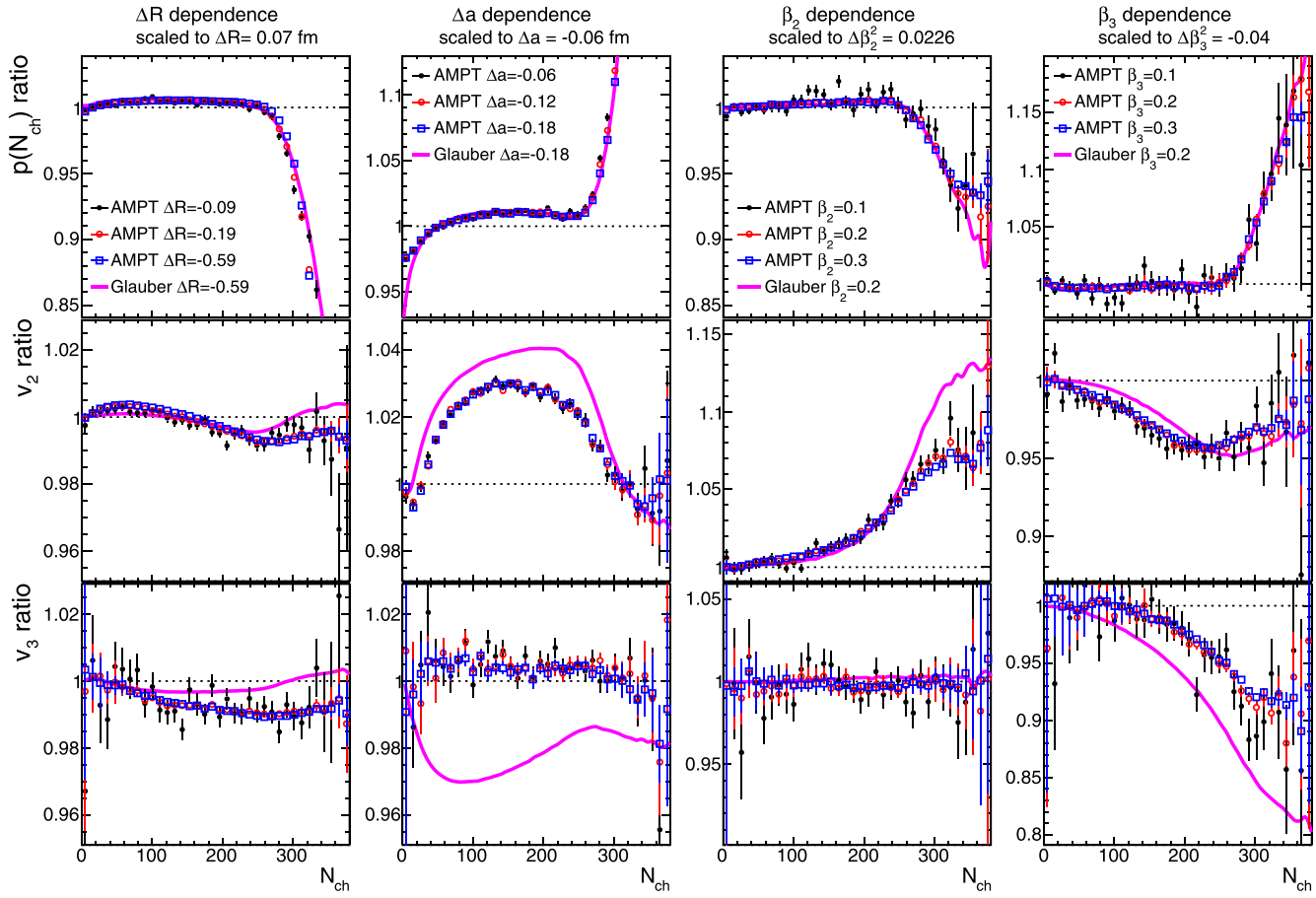

FIG. 2. The four terms of Eq. (3) associated with R_0 (left column), a (second column), β_2 (third column), and β_3 (right column) from the AMPT model for ratios of $p(N_{\rm ch})$ (first row), v_2 (middle row), and v_3 (bottom row). Distribution in each panel is determined for several values of parameters and scaled to the same default value. They are compared with those obtained for quark Glauber model (solid lines).

peripheral collisions, the impact of Δa is more important; 4) the influence of ΔR_0 is negligible except in central collisions. Lastly, the ratio $v_{3,\rm Ru}/v_{3,\rm Zr}$ is mainly influenced by $\Delta\beta_3^2$, although Δa and ΔR_0 have opposite up to 1% contributions over a broad $N_{\rm ch}$ range.

The scaling relation in Fig. 2 allows us to construct directly the ratios of experimental observables for any values of $\Delta\beta_2^2$, $\Delta\beta_3^2$, Δa, and ΔR_0, without the need to carry out additional simulations. One could also perform a simultaneous fit of several experimental ratios to obtain the optimal values of these parameters within a given model framework and expose its limitations. Figure 3 shows a step-by-step construction of the prediction in comparison with the STAR data. Each panel also shows the ratio obtained directly from a separate AMPT simulation of ^{96}Ru+^{96}Ru and ^{96}Zr+^{96}Zr collisions using the default parameters in the Table I. Excellent agreement is obtained between the construction approach and the direct calculation, attesting to the robustness of our proposed method. Also for the first time, we achieved simultaneous description of all three ratios using one set of WS parameters in most centrality ranges.

One natural question is how these isobar ratios are influenced by various final state effects. A recent study from us has demonstrated explicitly that isobar ratios are insensitive to the shear viscosity, hadronization, and hadronic transport [33]. Therefore, any model dependence in the isobar ratios must reflect a model dependence in the initial condition, i.e., how the energy is deposited in the overlap region (see Fig. 1). One example is the response functions calculated from a quark Glauber model shown in Fig. 2 (details in the Supplemental Material [54]), which has clear differences in several cases from the AMPT model. There are potentially many initial conditions, reflected by the well-known T$_{\rm R}$ENTo formula for the energy density $e(x,y) \propto (T_{\rm A}^p + T_{\rm B}^p)^{q/p}$ calculated from the thickness function $T_{\rm A}$ and $T_{\rm B}$ of colliding ions, where each q and p value specify a different initial condition [56,57]. The coefficients c_n provide a new way to constrain the initial condition by exploiting structure differences between isobars. One has to first calibrate the values of c_n using species whose WS parameters are relatively well known. The calibrated c_n can then be used to 1) narrow the q and p values, which can be subsequently fixed in the Bayesian inference to improve the extraction of the QGP properties, and 2) constrain the nuclear structure parameters for species of interest by directly fitting Eq. (3) to the measured isobar ratios.

A caveat is in order regarding to the connection between nuclear structure and initial condition. The parameters describing the shape of the nuclei in high energy may not take

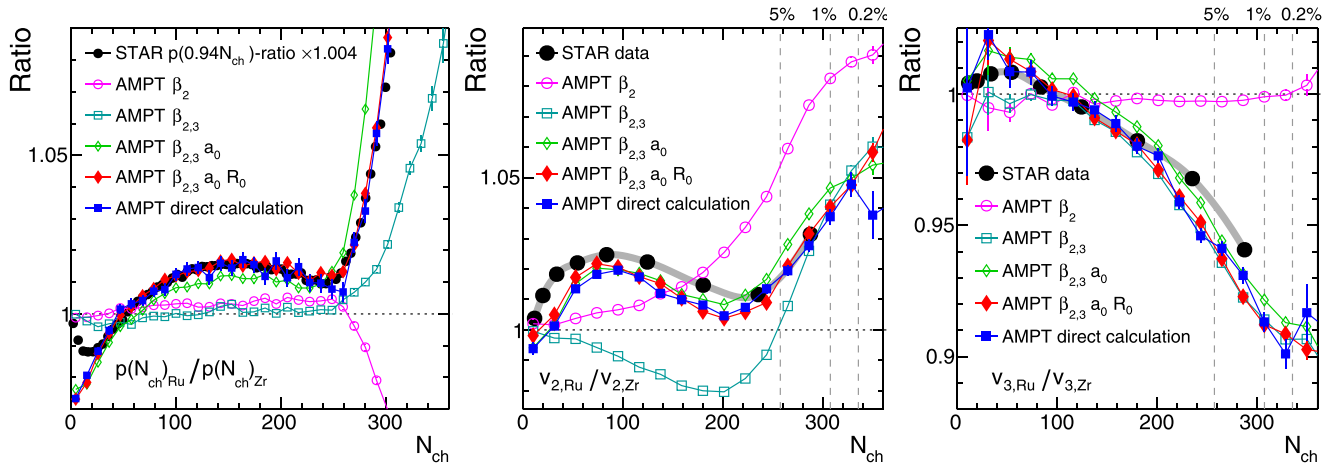

FIG. 3. The ratios of $p(N_{\rm ch})$ (left), v_2 (middle), and v_3 (right) from AMPT using the default nuclear structure parameters in Table I (labeled "direct calculation") or calculated step by step from the response coefficients from Fig. 2. The $N_{\rm ch}$ and $R_{p(N_{\rm ch})}$ values from data have been scaled by 0.94 and 1.004, respectively, to match the AMPT. Note also that the STAR v_n ratios at the same centrality [41] have been corrected to reflect the ratio at the same $N_{\rm ch}$ [53].

the same values as those at low energy. In fact, nuclear structure at small partonic longitudinal momentum fraction (small x), is expected to be modified due to gluon shadowing or saturation effects, described by the nuclear partonic distribution function (nPDF). The nPDF appears as additional spatial modulation of the nucleon distribution in the transverse plane, and will modify the values of the parameters in Eq. (1) in a x-dependent way. The nPDF effects, as input to the heavy-ion initial condition, is a key topic in $e+A$ collisions at future electron-ion collider (EIC) and $p+A$ collisions. The isobar collisions provide a new means to access modification of nuclear structure in dense gluon environment in a data-driven approach, for example by comparing isobar ratios between the RHIC and the LHC energies or as a function of rapidity.

The scaling approach discussed above can be extended to compare collisions of systems with similar but slightly different mass number A, ideally along an isotopic chain. As the $N_{\rm ch}$ distribution scales approximately with A, the ratios of experimental observable can be obtained as a function of $N_{\rm ch}/(2A)$ or centrality. In this case, one has $b_0 \to b_0(1+\frac{d\ln b_0}{d\ln A}\frac{\Delta A}{A})$, which leads to one additional term, $\frac{d\ln b_0}{d\ln A}\frac{\Delta A}{A}$, in Eq. (3). The A dependence of c_n is weak and also its contribution to Eq. (3) has a higher-order form, e.g., $\frac{\Delta A}{A}\Delta a$, etc., therefore is ignored. Studies along this line have been done for elliptic flow [18,20], which show that the b_0 for ϵ_2 has the form $b_0 \propto 1/A$ in the ultracentral collisions, and that R_{ϵ_2} receives an additional correction $-\Delta A/A$. This contribution should be quantified for each observable and compared to data from two systems of similar sizes, such as ^{197}Au $+^{197}$Au and ^{238}U $+^{238}$U. In conjunction with the scaling relations for the nuclear structure parameters discussed above, they can be a powerful tool in understanding the system size dependence of heavy-ion observables.

The scaling approach also provides a clean way to probe the difference between the root mean square radius of neutrons and protons in heavy nuclei, $\Delta r_{np} = R_n - R_p$, known as the neutron skin. The Δr_{np} is related to the symmetry energy contribution to the equation of state (EOS): a quantity of fundamental importance in nuclear- and astrophysics [58,59]. From the discussion above, the isobar ratios are expected to probe only the difference in the neutron skin. To see this, we first express the mean square radius of nucleon distribution in Eq. (1) by $R^2 \approx (\frac{3}{5}R_0^2 + \frac{7}{5}\pi^2 a^2)/(1+\frac{5}{4\pi}\sum_n \beta_n^2)$ [60]. The neutron skin is then expressed in terms of the differences between nucleon distribution and proton distribution

$$\Delta r_{np} = \frac{R^2 - R_p^2}{R(\delta+1)} \approx \frac{3\left(R_0^2 - R_{0,p}^2\right) + 7\pi^2\left(a^2 - a_p^2\right)}{\sqrt{15}R_0\sqrt{1+\frac{7\pi^2}{3}\frac{a^2}{R_0^2}}\left(1+\delta+\frac{5}{8\pi}\sum_n \beta_n^2\right)}, \tag{4}$$

where $\delta = (N-Z)/A$, and $R_{0,p}$ and a_p are the well-measured WS parameters for the proton distribution [50]. Simple algebraic manipulation shows that ΔR_0 and Δa are related to the skin difference [54],

$$\Delta(\Delta r_{np}) \approx -\overline{\Delta r}_{np}\left(\frac{\Delta\delta}{1+\bar{\delta}} + \frac{\Delta R_0}{\bar{R}_0}\right) + \frac{\Delta Y - \frac{7\pi^2}{6}\frac{\bar{a}^2}{\bar{R}_0^2}\left(\Delta Y + 2\bar{Y}\left(\frac{\Delta a}{\bar{a}} - \frac{\Delta R_0}{\bar{R}_0}\right)\right)}{\sqrt{15}\bar{R}_0\left(1+\bar{\delta}+\frac{5}{8\pi}\sum_n \overline{\beta_n^2}\right)}, \tag{5}$$

where $\bar{x}$ represents the average of x between the two systems, and $Y \equiv 3(R_0^2 - R_{0,p}^2) + 7\pi^2(a^2 - a_p^2)$. The term associated with $\overline{\Delta r}_{np}$ can be dropped if we ignore change of δ and R_0, which is typically a few percents of $\overline{\Delta r}_{np}$ for isobar systems. The numerator of Eq. (5) is dominated by $\Delta Y = 6(\bar{R}_0\Delta R_0 - \bar{R}_{0p}\Delta R_{0p}) + 14\pi^2(\bar{a}\Delta a - \bar{a}_p\Delta a_p)$, the remaining term is on the order of $\frac{7\pi^2}{6}\frac{\bar{a}^2}{\bar{R}_0^2} \approx 11(0.5/5)^2 = 11\%$ of ΔY. We checked that Eq. (5) is accurate within 2% using parameters for ^{96}Ru and ^{96}Zr listed in Ref. [49].

Knowledge of nucleon distribution gives direct information on the neutron skin, once it is combined with the well-known proton distribution. Equation (5) shows that isobar data can

only constrain the neutron skin difference, which can be constructed from ΔR_0 and Δa, together with well-measured $\Delta R_{0,p}$ and Δa_p for protons. The neutron skin difference is sensitive to both ΔR_0 (skin-type contribution) and Δa (halo-type contribution) [51,61]. Previous studies of neutron skin are done by inputting density functional theory (DFT) calculation of nuclear structure directly to the hydrodynamic modeling of heavy-ion collisions [34,49,62]. The neutron skin values are constrained by comparing directly with experimental observables. What we are proposing here is to decouple DFT from modeling of heavy-ion collisions. One first extracts the ΔR_0 and Δa values consistent with many isobar ratios using the scaling approach, which are then compared with those calculated directly from nucleon distributions from the DFT theory. Equation (5) provides an easy way to estimate the skin difference, and contributions from skin-type or halo-type.

In summary, we presented a new approach to constrain the collective nuclear structure parameters in high-energy heavy-ion isobar collisions. We found that the changes in the final state observables $v_2(N_{\rm ch})$, $v_3(N_{\rm ch})$, and $p(N_{\rm ch})$ follow a simple dependence on the variation of these parameters. The coefficients of these variations can be determined precisely in a given model framework, and subsequently used to make predictions of observables at other parameter values. This scaling behavior is particularly useful in analyzing the ratios between isobar systems, such as ^{96}Ru+^{96}Ru and ^{96}Zr+^{96}Zr collisions measured by the STAR experiment [41]. We show that the STAR data can constrain directly the nuclear structure differences between ^{96}Ru and ^{96}Zr (compatible with the structure values in Table I). Since these isobar ratios are also found to be insensitive to the details of interaction in the final state, the isobar collisions serve as a precise tool for accessing both the bulk nuclear structure parameters and the initial condition of heavy-ion collisions. The extracted information on nucleon distribution, together with well-measured charge distribution, can probe the difference in the neutron skin between large isobar systems. However, future measurements of isobar ratios as a function of collision energy and rapidity, are necessary to quantify the modification of nuclear structure at high-energy across energy scales, and establish more firmly the connection between nuclear structure and the initial condition. Our study demonstrates the unique opportunities offered by relativistic collisions of isobars as a tool to perform interdisciplinary nuclear physics studies, which we hope will be pursued in future by collisions of several isobar pairs in collider facilities.

We thank Giuliano Giacalone, Che-Ming Ko, Bao-An Li, and Jun Xu for a careful reading and valuable comments on the manuscript. This work is supported by DOE DE-FG02-87ER40331.

[1] T. Nakatsukasa, K. Matsuyanagi, M. Matsuo, and K. Yabana, Time-dependent density-functional description of nuclear dynamics, Rev. Mod. Phys. **88**, 045004 (2016).
[2] W. Nazarewicz, Challenges in nuclear structure theory, J. Phys. G: Nucl. Part. Phys. **43**, 044002 (2016).
[3] P. Möller, A. J. Sierk, T. Ichikawa, and H. Sagawa, Nuclear ground-state masses and deformations: FRDM(2012), At. Data Nucl. Data Tables **109–110**, 1 (2016).
[4] Y. Cao, S. E. Agbemava, A. V. Afanasjev, W. Nazarewicz, and E. Olsen, Landscape of pear-shaped even-even nuclei, Phys. Rev. C **102**, 024311 (2020).
[5] I. Angeli and K. P. Marinova, Table of experimental nuclear ground state charge radii: An update, At. Data Nucl. Data Tables **99**, 69 (2013).
[6] M. Centelles, X. Roca-Maza, X. Vinas, and M. Warda, Nuclear Symmetry Energy Probed by Neutron Skin Thickness of Nuclei, Phys. Rev. Lett. **102**, 122502 (2009).
[7] I. Tanihata, H. Hamagaki, O. Hashimoto, Y. Shida, N. Yoshikawa, K. Sugimoto, O. Yamakawa, T. Kobayashi, and N. Takahashi, Measurements of Interaction Cross-Sections and Nuclear Radii in the Light p Shell Region, Phys. Rev. Lett. **55**, 2676 (1985).
[8] A. Rosenhauer, H. Stocker, J. A. Maruhn, and W. Greiner, Influence of shape fluctuations in relativistic heavy ion collisions, Phys. Rev. C **34**, 185 (1986).
[9] B.-A. Li, Uranium on uranium collisions at relativistic energies, Phys. Rev. C **61**, 021903(R) (2000).
[10] U. W. Heinz and A. Kuhlman, Anisotropic Flow and Jet Quenching in Ultrarelativistic U + U Collisions, Phys. Rev. Lett. **94**, 132301 (2005).
[11] P. Filip, R. Lednicky, H. Masui, and N. Xu, Initial eccentricity in deformed ^{197}Au+^{197}Au and ^{238}U+^{238}U collisions at $\sqrt{s_{NN}} = 200$ GeV at the BNL Relativistic Heavy Ion Collider, Phys. Rev. C **80**, 054903 (2009).
[12] Q. Y. Shou, Y. G. Ma, P. Sorensen, A. H. Tang, F. Videbæk, and H. Wang, Parameterization of deformed nuclei for Glauber modeling in relativistic heavy ion collisions, Phys. Lett. B **749**, 215 (2015).
[13] A. Goldschmidt, Z. Qiu, C. Shen, and U. Heinz, Collision geometry and flow in uranium + uranium collisions, Phys. Rev. C **92**, 044903 (2015).
[14] G. Giacalone, J. Noronha-Hostler, M. Luzum, and J.-Y. Ollitrault, Hydrodynamic predictions for 5.44 TeV Xe+Xe collisions, Phys. Rev. C **97**, 034904 (2018).
[15] G. Giacalone, Observing the Deformation of Nuclei with Relativistic Nuclear Collisions, Phys. Rev. Lett. **124**, 202301 (2020).
[16] G. Giacalone, Constraining the quadrupole deformation of atomic nuclei with relativistic nuclear collisions, Phys. Rev. C **102**, 024901 (2020).
[17] G. Giacalone, J. Jia, and V. Somà, Accessing the shape of atomic nuclei with relativistic collisions of isobars, Phys. Rev. C **104**, L041903 (2021).
[18] G. Giacalone, J. Jia, and C. Zhang, Impact of Nuclear Deformation on Relativistic Heavy-Ion Collisions: Assessing Consistency in Nuclear Physics across Energy Scales, Phys. Rev. Lett. **127**, 242301 (2021).
[19] J. Jia, S. Huang, and C. Zhang, Probing nuclear quadrupole deformation from correlation of elliptic flow and transverse momentum in heavy ion collisions, Phys. Rev. C **105**, 014906 (2022).

[20] J. Jia, Shape of atomic nuclei in heavy ion collisions, Phys. Rev. C **105**, 014905 (2022).

[21] B. Bally, M. Bender, G. Giacalone, and V. Somà, Evidence of the Triaxial Structure of ^{129}Xe at the Large Hadron Collider, Phys. Rev. Lett. **128**, 082301 (2022).

[22] L. Adamczyk *et al.* (STAR Collaboration), Azimuthal Anisotropy in U+U and Au+Au Collisions at RHIC, Phys. Rev. Lett. **115**, 222301 (2015).

[23] S. Acharya *et al.* (ALICE Collaboration), Anisotropic flow in Xe-Xe collisions at $\sqrt{s_{\rm NN}} = 5.44$ TeV, Phys. Lett. B **784**, 82 (2018).

[24] A. M. Sirunyan *et al.* (CMS Collaboration), Charged-particle angular correlations in XeXe collisions at $\sqrt{s_{\rm NN}} = 5.44$ TeV, Phys. Rev. C **100**, 044902 (2019).

[25] G. Aad *et al.* (ATLAS Collaboration), Measurement of the azimuthal anisotropy of charged-particle production in $Xe + Xe$ collisions at $\sqrt{s_{\rm NN}} = 5.44$ TeV with the ATLAS detector, Phys. Rev. C **101**, 024906 (2020).

[26] J. Jia, Nuclear deformation effects via Au+Au and U+U collisions from STAR, Contribution to the VIth International Conference on the Initial Stages of High-Energy Nuclear Collisions, January 2021, https://indico.cern.ch/event/854124/contributions/4135480/.

[27] W. Busza, K. Rajagopal, and W. van der Schee, Heavy ion collisions: The big picture, and the big questions, Annu. Rev. Nucl. Part. Sci. **68**, 339 (2018).

[28] D. Teaney and L. Yan, Non linearities in the harmonic spectrum of heavy ion collisions with ideal and viscous hydrodynamics, Phys. Rev. C **86**, 044908 (2012).

[29] H. Niemi, K. J. Eskola, and R. Paatelainen, Event-by-event fluctuations in a perturbative QCD + saturation + hydrodynamics model: Determining QCD matter shear viscosity in ultrarelativistic heavy-ion collisions, Phys. Rev. C **93**, 024907 (2016).

[30] W. Horiuchi, Single-particle decomposition of nuclear surface diffuseness, PTEP (2021) 123D01.

[31] P. Carzon, S. Rao, M. Luzum, M. Sievert, and J. Noronha-Hostler, Possible octupole deformation of ^{208}Pb and the ultracentral v_2 to v_3 puzzle, Phys. Rev. C **102**, 054905 (2020).

[32] H. Li, H.-j. Xu, J. Zhao, Z.-W. Lin, H. Zhang, X. Wang, C. Shen, and F. Wang, Multiphase transport model predictions of isobaric collisions with nuclear structure from density functional theory, Phys. Rev. C **98**, 054907 (2018).

[33] C. Zhang, S. Bhatta, and J. Jia, Ratios of collective flow observables in high-energy isobar collisions are insensitive to final-state interactions, Phys. Rev. C **106**, L031901 (2022).

[34] H.-j. Xu, W. Zhao, H. Li, Y. Zhou, L.-W. Chen, and F. Wang, Probing nuclear structure with mean transverse momentum in relativistic isobar collisions, arXiv:2111.14812 [nucl-th] (2021).

[35] S. Zhao, H.-j. Xu, Y.-X. Liu, and H. Song, Probing the nuclear deformation with three-particle asymmetric cumulant in RHIC isobar runs, arXiv:2204.02387 [nucl-th] (2022).

[36] J. Jia, G. Giacalone, and C. Zhang, Precision tests of the nonlinear mode coupling of anisotropic flow via high-energy collisions of isobars, arXiv:2206.07184 [nucl-th] (2022).

[37] J. Jia, G. Giacalone, and C. Zhang, Separating the impact of nuclear skin and nuclear deformation on elliptic flow and its fluctuations in high-energy isobar collisions, arXiv:2206.10449 [nucl-th] (2022).

[38] J. E. Bernhard, J. S. Moreland, S. A. Bass, J. Liu, and U. Heinz, Applying Bayesian parameter estimation to relativistic heavy-ion collisions: Simultaneous characterization of the initial state and quark-gluon plasma medium, Phys. Rev. C **94**, 024907 (2016).

[39] D. Everett *et al.* (JETSCAPE Collaboration), Multisystem Bayesian constraints on the transport coefficients of QCD matter, Phys. Rev. C **103**, 054904 (2021).

[40] G. Nijs, W. van der Schee, U. Gürsoy, and R. Snellings, Transverse Momentum Differential Global Analysis of Heavy-Ion Collisions, Phys. Rev. Lett. **126**, 202301 (2021).

[41] M. Abdallah *et al.* (STAR Collaboration), Search for the chiral magnetic effect with isobar collisions at $\sqrt{s_{NN}}$=200 GeV by the STAR Collaboration at the BNL relativistic heavy ion collider, Phys. Rev. C **105**, 014901 (2022).

[42] J. Jia, Probing triaxial deformation of atomic nuclei in high-energy heavy ion collisions, Phys. Rev. C **105**, 044905 (2022).

[43] Z.-W. Lin, C. M. Ko, B.-A. Li, B. Zhang, and S. Pal, A Multi-phase transport model for relativistic heavy ion collisions, Phys. Rev. C **72**, 064901 (2005).

[44] J. Xu and C. M. Ko, Pb-Pb collisions at $\sqrt{s_{NN}} = 2.76$ TeV in a multiphase transport model, Phys. Rev. C **83**, 034904 (2011).

[45] M. Abdallah *et al.* (STAR Collaboration), Azimuthal anisotropy measurements of strange and multistrange hadrons in $U + U$ collisions at $\sqrt{s_{NN}}$ =193 GeV at the BNL relativistic heavy ion collider, Phys. Rev. C **103**, 064907 (2021).

[46] C. Zhang and J. Jia, Evidence of Quadrupole and Octupole Deformations in ^{96}Zr + ^{96}Zr and ^{96}Ru + ^{96}Ru Collisions at Ultrarelativistic Energies, Phys. Rev. Lett. **128**, 022301 (2022).

[47] G.-L. Ma and A. Bzdak, Long-range azimuthal correlations in proton-proton and proton-nucleus collisions from the incoherent scattering of partons, Phys. Lett. B **739**, 209 (2014).

[48] A. Bzdak and G.-L. Ma, Elliptic and triangular flow in p+Pb and peripheral Pb+Pb collisions from parton scatterings, Phys. Rev. Lett. **113**, 252301 (2014).

[49] H.-j. Xu, H. Li, X. Wang, C. Shen, and F. Wang, Determine the neutron skin type by relativistic isobaric collisions, Phys. Lett. B **819**, 136453 (2021).

[50] G. Fricke, C. Bernhardt, K. Heilig, L. A. Schaller, L. Schellenberg, E. B. Shera, and C. W. de Jager, Nuclear ground state charge radii from electromagnetic interactions, At. Data Nucl. Data Tables **60**, 177 (1995).

[51] A. Trzcinska, J. Jastrzebski, P. Lubinski, F. J. Hartmann, R. Schmidt, T. von Egidy, and B. Klos, Neutron Density Distributions Deduced from Antiprotonic Atoms, Phys. Rev. Lett. **87**, 082501 (2001).

[52] G. Aad *et al.* (ATLAS Collaboration), Measurement of the azimuthal anisotropy for charged particle production in $\sqrt{s_{\rm NN}} =$ 2.76 TeV lead-lead collisions with the ATLAS detector, Phys. Rev. C **86**, 014907 (2012).

[53] J. Jia, G. Wang, and C. Zhang, Impact of event activity variable on the ratio of observables in isobar collisions, Phys. Lett. B **833**, 137312 (2022).

[54] See Supplemental Material at http://link.aps.org/supplemental/10.1103/PhysRevC.107.L021901 for a derivation of Eq. (5) and scaling behavior observed in the Glauber model which can be compared with Fig. 2.

[55] D. Everett *et al.* (JETSCAPE Collaboration), Phenomenological Constraints on the Transport Properties of QCD Matter with

Data-Driven Model Averaging, Phys. Rev. Lett. **126**, 242301 (2021).

[56] J. S. Moreland, J. E. Bernhard, and S. A. Bass, Alternative ansatz to wounded nucleon and binary collision scaling in high-energy nuclear collisions, Phys. Rev. C **92**, 011901(R) (2015).

[57] G. Nijs and W. van der Schee, Hadronic Nucleus-Nucleus Cross Section and the Nucleon Size, Phys. Rev. Lett. **129**, 232301 (2022).

[58] J. M. Lattimer and M. Prakash, Neutron Star Observations: Prognosis for Equation of State Constraints, Phys. Rep. **442**, 109 (2007).

[59] B.-A. Li, L.-W. Chen, and C. M. Ko, Recent Progress and New Challenges in Isospin Physics with Heavy-Ion Reactions, Phys. Rep. **464**, 113 (2008).

[60] *Nuclear Structure* edited by A. Bohr and B. R Mottelson (World Scientific, New York, 1998).

[61] M. Centelles, X. Roca-Maza, X. Vinas, and M. Warda, Origin of the neutron skin thickness of ^{208}Pb in nuclear mean-field models, Phys. Rev. C **82**, 054314 (2010).

[62] H. Li, H.-j. Xu, Y. Zhou, X. Wang, J. Zhao, L.-W. Chen, and F. Wang, Probing the Neutron Skin with Ultrarelativistic Isobaric Collisions, Phys. Rev. Lett. **125**, 222301 (2020).